



Research Article

Structural and Optical Characterization of Cadmium Ferrite and Manganese Ferrite Nanoparticles synthesized via Co-precipitation route

Remya Muralimanohar ^a, Anu Jyothi S ^a, Arya Sreekumar ^a Saravana Kumar S ^{a*}

^a Department of Physics, N S S College, Pandalam, Kerala 689501, India

*Corresponding author (E-mail address: saravanks80@gmail.com)

Received: 16/11/2022, Received in revised form: 12/02/2023, Accepted: 19/03/2023

Abstract

Spinel ferrite nanoparticles have been of tremendous interest in the arena of nanomaterial synthesis and has applications comprising industrial effluent treatment, as biosensors and for photocatalysis. Cadmium ferrite and manganese ferrite nanoparticles have been in the limelight recently due to their versatile applications. In the present work, nanoparticles of cadmium ferrite and manganese ferrite were synthesized using chemical precipitation method and were calcined at 600 °C and 1000 °C. It was observed from the XRD pattern that the samples were in normal spinel structure. The grain size of the samples was calculated using Debye-Scherrer as well as Hall-Williamson method. The optical band gap was calculated from UV-Visible absorption spectrum. The vibrational properties of the samples were studied using micro-Raman technique.

Keywords: Spinel ferrites, co-precipitation method, magnetic nanoparticles, grain size, band gap

1. Introduction

Ferrites are a group of magnetic oxide [1] compounds that has iron oxide as the basic building block. Spinel Ferrite Nanoparticles with a general formula AFe_2O_4 can be fabricated in varied morphologies by altering the synthesis routes. Still, they maintain the unique properties of their spinel structure like high chemical and thermal stability, catalytic action and magnetic behaviour [2, 3].

Cadmium ferrite nanoparticles ($CdFe_2O_4$) are normal spinel ferrite structures with immense physico-chemical attributes. $CdFe_2O_4$ nanoparticles exhibit ferromagnetism, and approximately 54% of Fe^{3+} ions occupy the A site in contrast to 0% for the bulk materials with normal spinel structures [4]. A higher octahedral preferential energy of Cd^{2+} is responsible for the enhanced occupancy of Fe^{3+} ions in $CdFe_2O_4$. Cadmium ferrite nanoparticles find applications in the fields of sensors, catalysis and magnetic technologies. Manganese ferrite ($MnFe_2O_4$) nanoparticles are magnetic metal oxide nanoparticles with very novel physical and chemical properties which makes itself an impressive candidate for usage in storage devices, biomedical and electronics applications [5-11].

A proper selection of synthesis route should be made based on the knowhow in crystal chemistry to obtain tailor-made physical, electrical and catalytic properties. SNPs are formulated in different methods of which co precipitation method is the fastest and most economic one that can achieve uniform particle sizes. One major limitation of this method is,

it necessitates subsequent thermal treatment to obtain better crystallinity [12]. Other methods used for the fabrication of SNPs include microemulsion[13], ultrasonic [14,15], solvothermal [16-19], mechanical milling [20], combustion [21], reverse micelle [22], spray pyrolysis [23], electrospinning [24], self-reactive quenching [25], double sintering ceramics [26], powder metallurgy [27], self-propagating high temperature [28], thermal decomposition [29], liquid exchange [30], sol-gel [31] and solid-state reaction [32].

In the present work, cadmium ferrite and manganese ferrite nanoparticles were synthesized by chemical precipitation method. The samples were calcined at 600 °C and 1000 °C. Structural characterization was done by X-ray diffraction method and grain size was calculated using Debye- Scherrer equation and Hall-Williamson method. The optical properties of the samples were studied using UV-Visible absorption spectra and the band gap was calculated from Tauc's plot. The vibrational properties of the samples were analyzed using micro-Raman Spectroscopy.

2. Materials and Methods

2.1 Materials

CdFe₂O₄ and MnFe₂O₄ nanoparticles were synthesized by arrested precipitation method with cadmium sulphate and manganous sulphate as the cadmium and manganese sources respectively. Ferrous sulphate and Sodium Hydroxide were used as Iron and Oxygen sources and glycine as the capping agent. Deionised water was used as the solvent. All reagents were of analytical grade and used without further purification.

2.2 Methods

10ml, 3 M aqueous solution of NaOH was taken in a 250 ml beaker into which 65 ml of distilled water was added by continuous stirring using a magnetic stirrer. After stirring for 5 minutes 5 ml glycine was added as the capping agent. While continuing the process of stirring, 10 ml, 0.2 M of cadmium sulphate and 10 ml, 0.4 M of ferrous sulphate were added. The solution was then heated to 80 °C and stirred for 30 minutes. The precipitate was extracted through centrifuging it for five times at 5000 rpm for 20 minutes each. The separated precipitate was washed with distilled water and acetone. The sample was then dried and it was grinded using agate mortar. The sample was then annealed at 600 °C to obtain CdFe₂O₄ nanoparticles. Similar method was employed for the synthesis of MnFe₂O₄ Nanoparticles by substituting Cadmium sulphate with Manganous sulphate.

3. Results and Discussion

3.1 X Ray Diffraction

X-ray diffraction patterns of the nanoparticles of cadmium iron oxide and manganese iron oxide were recorded using a PANalytical 3 kW X'Pert PRO X-ray diffractometer with CuK α radiation ($\lambda = 1.5418 \text{ \AA}$) source over the diffraction angle, 2θ , between 10 °C and 80 °C. The X-ray diffraction pattern of nanoparticles [33-36] of CdFe₂O₄ calcined at 600 °C and 1000 °C are shown in the figures 3.1.1a and 3.1.1b respectively.

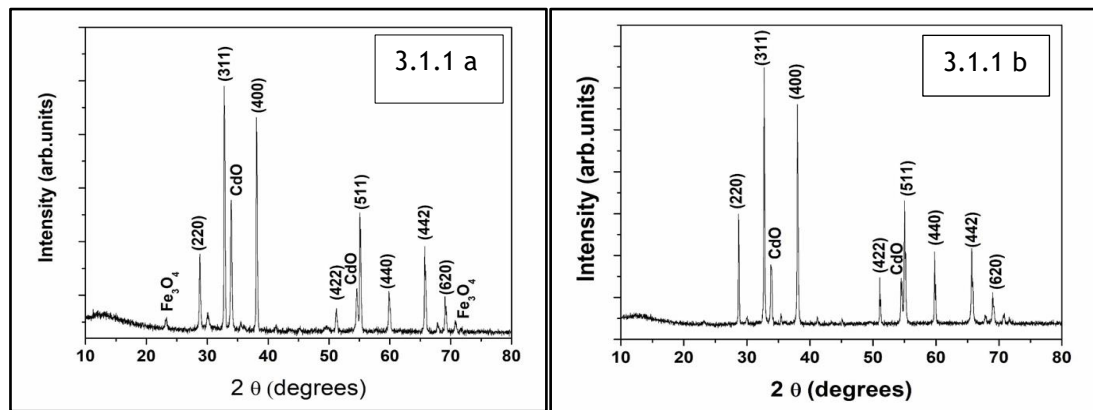


Figure 3.1.1a & 3.1.1b: XRD pattern of CdFe₂O₄ nanoparticles calcined at 600^oC and 1000^oC respectively

The d-value corresponding to each peak in the XRD pattern was calculated and compared with the standard JCPDS (Card No. 22-1063) values for CdFe₂O₄ [37]. The patterns imply the formation of cubic crystal structure. The XRD pattern of CdFe₂O₄ nanoparticles calcined at 600^oC contained peaks corresponding to CdO and Fe₃O₄. On calcining at 1000^oC, the peak at 23.2^oC corresponding to Fe₃O₄ was absent and the intensity of the peaks corresponding to CdO phases were reduced. The broad peaks of X-ray diffraction patterns suggest that the particles of the synthesized samples are in nanometer range. The 2θ values, d-values and corresponding reflection planes are listed in table 3.1.

Table 3.1. The 2θ values, corresponding d-values and reflection planes of CdFe₂O₄ nanoparticles

2θ(degrees)	d-spacing [Å]	Planes
23.25	3.82	Fe ₃ O ₄
28.72	3.12	(220)
32.61	2.74	(311)
33.84	2.65	CdO
38.09	2.36	(400)
50.98	1.79	(422)
54.51	1.68	CdO
54.69	1.66	(511)
59.82	1.54	(440)
65.64	1.42	(442)
69.17	1.36	(620)

The X-ray diffraction patterns of nanoparticles of MnFe₂O₄ calcined at 600^oC and 1000^oC are shown in the figures 3.1.2a and 3.1.2b respectively. The d-value corresponding to each peak in the XRD pattern was calculated and compared with the standard JCPDS (Card No. 74-2403) values for MnFe₂O₄ [37]. The patterns show the formation of cubic crystal structure. The XRD spectrum of MnFe₂O₄ nanoparticles calcined at 600^oC contained peaks due to MnO phase also. On calcination at 1000^oC, the XRD peaks due to MnO phase disappeared and a peak at 65.7^oC corresponding to reflection from (442) plane appeared. The broad peaks of X-

ray diffraction indicate the presence of nanosized particles. The 2θ values, d-values and corresponding reflection planes are listed in Table 3.2.

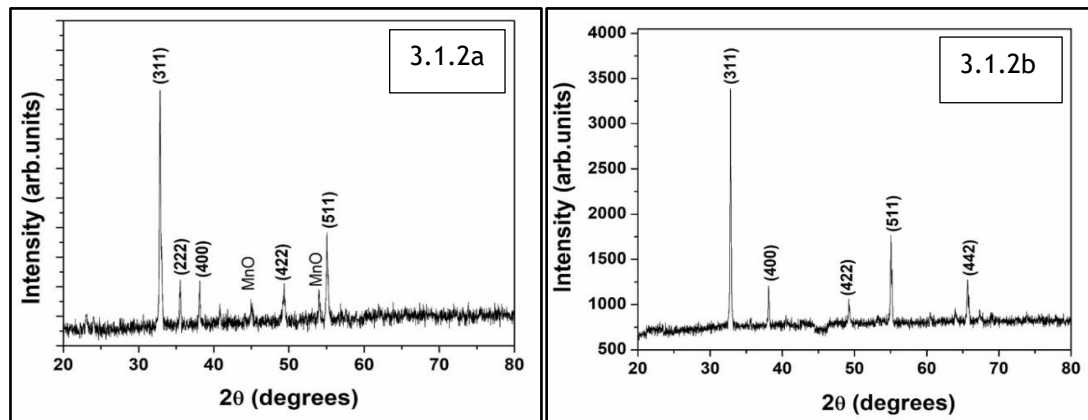


Figure 3.1.2a & 3.1.2b: XRD pattern of MnFe_2O_4 nanoparticles calcined at 600°C and 1000°C respectively

Table 3.2. The 2θ values, corresponding d-values and reflection planes of MnFe_2O_4 nanoparticles

2θ (degrees)	d-spacing [\AA]	Planes
32.89	2.72	(311)
35.65	2.52	(222)
38.17	2.35	(400)
44.99	2.01	MnO
49.52	1.85	(422)
53.72	1.72	MnO
55.13	1.66	(511)
65.57	1.42	(442)

Line broadening in the XRD pattern can be used to find grain size using Debye-Scherrer Equation.

$$D = k\lambda / \beta \cos\theta$$

where D is the mean grain size, k is a geometric factor (=0.89), λ is the X-ray wavelength, β is the FWHM of diffraction peak and θ is the diffraction angle. The grain sizes of the CdFe_2O_4 nanoparticles calcined at 600°C and 1000°C calculated from the most intense peak are 49 nm and 82 nm respectively; whereas those of MnFe_2O_4 stands at 40 nm and 49 nm respectively.

In the present study, Hall-Williamson method was used to calculate the grain size corresponding to zero strain of as-prepared CdFe_2O_4 and MnFe_2O_4 nanoparticles. In Hall and Williamson method, it is assumed that the two components of structural broadening i.e., size broadening and strain broadening are independent of each other and the observed width of broadening is the linear combination of these two factors [38,39]. According to Hall and Williamson, plotting the value of $\beta\cos\theta/\lambda$ as a function of $\sin\theta/\lambda$, the strain η may be estimated from the slope of the line and grain size corresponding to zero strain from the y intercept.

Figures 3.1.3a, 3.1.3b, 3.1.3c, 3.1.3d represent the plot of $\beta \cos\theta/\lambda$ versus $4\sin\theta/\lambda$ for the CdFe_2O_4 and MnFe_2O_4 nanoparticles of the present study calcined at 600°C and 1000°C respectively. The grain sizes of the as - prepared CdFe_2O_4 nanoparticles were found to be approximately 58 nm and 90 nm for the samples calcined at 600°C and 1000°C respectively whereas the value stands at 48 nm and 54 nm in the case of MnFe_2O_4 nanoparticles. Both the graphs exhibit a positive slope indicating tensile strain.

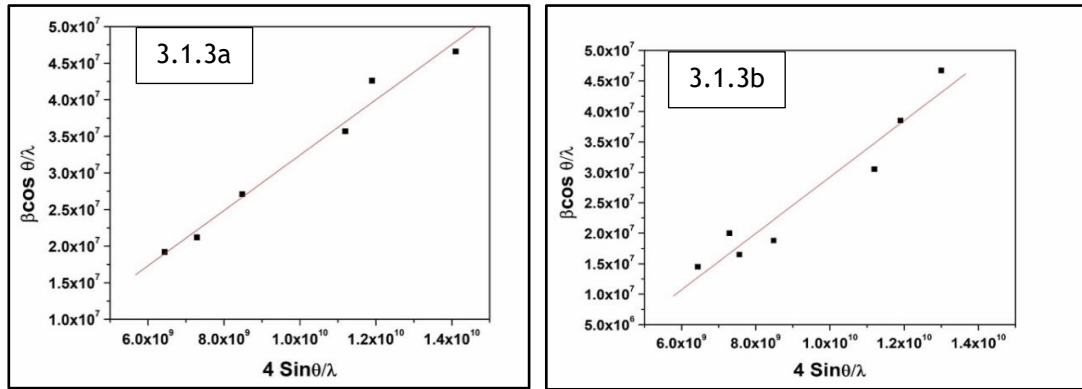


Figure 3.1.3a & 3.1.3b: Hall – Williamson Plot for nanoparticles of CdFe_2O_4 calcined at 600°C & 1000°C

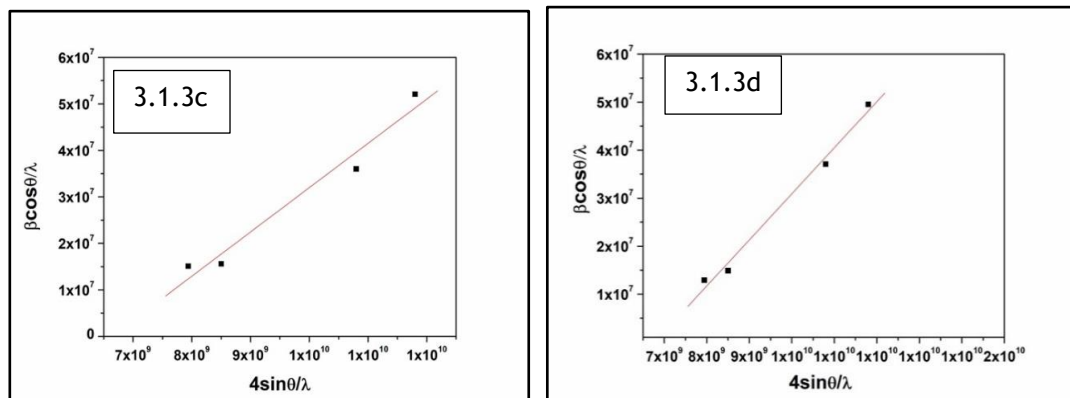


Figure 3.1.3c & 3.1.3d: Hall – Williamson Plot for nanoparticles of MnFe_2O_4 calcined at 600°C & 1000°C

The micro strain (ϵ) and the dislocation density (ρ) of the grown nanoparticles can be estimated using the following relations [40]

$$\text{Micro strain } \epsilon = \frac{\beta \cos \theta}{4} \quad \text{and}$$

$$\text{Dislocation density } \rho = \frac{1}{D^2}$$

Micro strain in nanoparticles describes the root mean square deviation of the lattice spacing from its mean value and it depends on the size. The micro strain and dislocation density of CdFe_2O_4 nanoparticles of present study are tabulated in table 3.3. From the tables, it can be observed that calcination at a temperature of 1000°C reduced strain and dislocation density. The higher temperature causes annihilation of dislocations with opposite Burger's vectors and absorption of dislocation at grain boundaries. In nanoscale, the grain boundaries reach more

equilibrium state and becomes sharper [41,42]. This further explains the temperature dependence of micro strain and dislocation density.

Table 3.3: Strain and dislocation density of CdFe₂O₄ Nanoparticles calcined at 600 °C and 1000 °C

Plane	Micro strain,	Dislocation Density,	Micro strain,	Dislocation Density,
	ϵ (*10 ⁻⁴) at 600 °C	ρ (*10 ¹² K gm. /cm ³) at 600 °C	ϵ (*10 ⁻⁴) at 1000 °C	ρ (*10 ¹² K gm. /cm ³) at 1000 °C
(311)	8.21	467	0.56	326
(400)	8.17	492	0.76	286
(422)	0.76	926	0.63	752
(511)	13.74	1610	0.59	833
(440)	1.64	2290	0.82	1789
(442)	11.54	1140	0.25	1013
(620)	19.36	3190	1.26	2875

The micro strain and dislocation density of MnFe₂O₄ nanoparticles of present study are tabulated in Table 3.4. From the tables, it can be observed that there is no considerable change in micro strain and dislocation density on calcination at higher temperatures.

Table 3.4: Strain and dislocation density of MnFe₂O₄ Nanoparticles calcined at 600 °C and 1000 °C

Plane	Micro strain,	Dislocation Density,	Micro strain,	Dislocation Density,
	ϵ (*10 ⁻⁴) at 600 °C	ρ (*10 ¹² K gm. /cm ³) at 600 °C	ϵ (*10 ⁻⁴) at 1000 °C	ρ (*10 ¹² K gm. /cm ³) at 1000 °C
(311)	8.42	608	8.03	549
(222)	2.52	288	4.98	211
(400)	6.02	308	5.73	279
(422)	13.88	1640	14.27	1740
(511)	10.44	928	8.51	616

3.2 UV - Visible Absorption Spectroscopy

In the present study, UV-visible spectrophotometer Systronics Type 117 which has a spectral range of 200 nm to 1100 nm is used. The absorption spectra of the nanoparticles of cadmium ferrite and manganese ferrite were recorded in the wavelength range from 200 nm to 800 nm. The samples were dispersed in ethanol to record absorption spectra.

Figure 3.2.1 shows the UV-Visible absorption spectrum and Tauc's plot of CdFe₂O₄ nanoparticles calcined at 600 °C. Figure 3.2.2 shows the UV-Visible absorption spectrum and Tauc's plot of cadmium ferrite nanoparticles calcined at 1000 °C. The band gap of cadmium ferrite calculated by extrapolating straight portion of the graph is found to be 2 eV. It is reported that bulk CdFe₂O₄ has a band gap of 1.83 eV. The band gap of nanoparticles is found to be increased due to quantum confinement effect which occurs when their grain sizes are

comparable with the bulk Bohr exciton radius. The band gap of nanoparticles of CdFe_2O_4 of present study showed blue shift compared to bulk band gap which may be attributed to quantum confinement effect [43,46]. The band gap of cadmium ferrite nanoparticles increased on calcination. The increase in band gap may be due to the orderly arrangement of crystal lattice on calcination [43].

There exists a significant difference in the absorption spectra of CdFe_2O_4 nanoparticles calcined at 1000°C from those calcined at 600°C . The broad absorption of the samples calcined at 600°C is due to the large size distribution. On annealing at 1000°C the size distribution becomes narrow and the absorption edge is shifted to higher wavelengths.

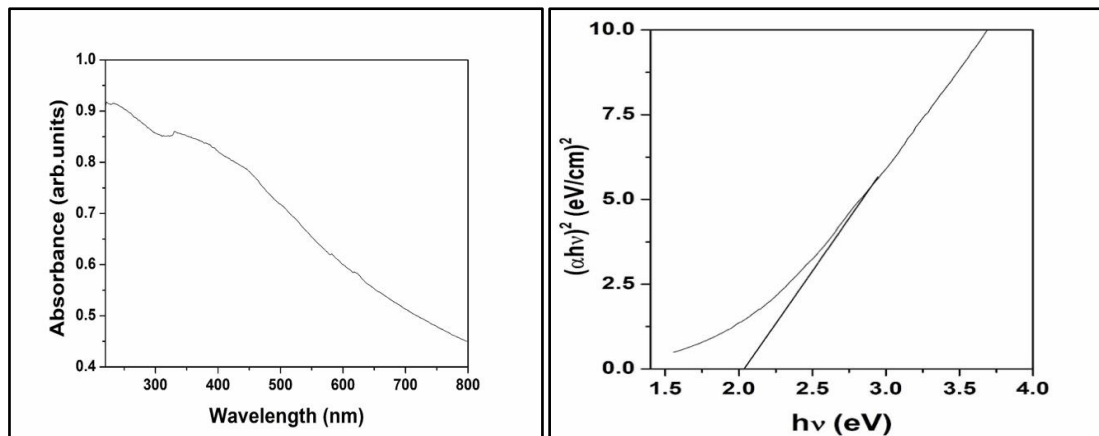


Figure 3.2.1: UV-Vis absorption spectrum and Tauc's plot of nanoparticles of CdFe_2O_4 calcined at 600°C .

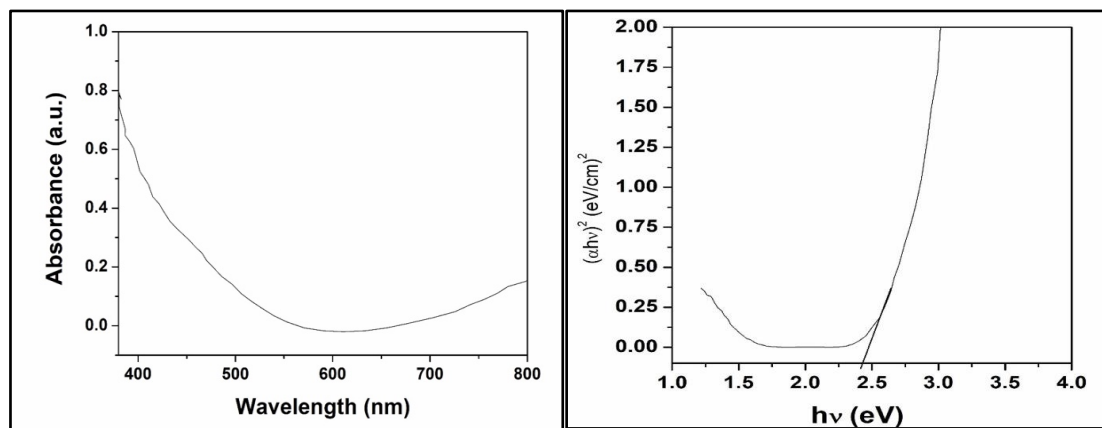


Figure 3.2.2 UV-Vis absorption spectrum and Tauc's plot of nanoparticles of CdFe_2O_4 calcined at 1000°C .

Figure 3.2.3 shows the UV-Visible absorption spectrum and Tauc's plot of manganese ferrite nanoparticles calcined at 600°C . The band gap of manganese ferrite calculated by extrapolating straight portion of the graph is found to 1.65 eV. It is reported that bulk MnFe_2O_4 has a band gap of 1.4 eV. The band gap of nanoparticles is found to be increased due to quantum confinement effect as a result of their grain sizes being comparable with the bulk Bohr exciton radius. The band gap of nanoparticles of MnFe_2O_4 of present study showed blue shift compared to bulk band gap which may be attributed to quantum confinement effect. The absorption spectrum of manganese ferrite nanoparticles calcined at 1000°C is shown in the figure 3.2.4.

A broad absorption band can be observed at around 717 nm, which indicates that the material can be used as a photocatalyst.

The absorption spectra of the MnFe_2O_4 nanoparticles calcined at $1000\text{ }^\circ\text{C}$ is conspicuously different from those calcined at $600\text{ }^\circ\text{C}$. A broad absorption peak in the higher wavelength region is due to the charge transfer transition. This occurs when the Mn^{2+} ions occupy the clear structural positions in the lattice due to calcination [47].

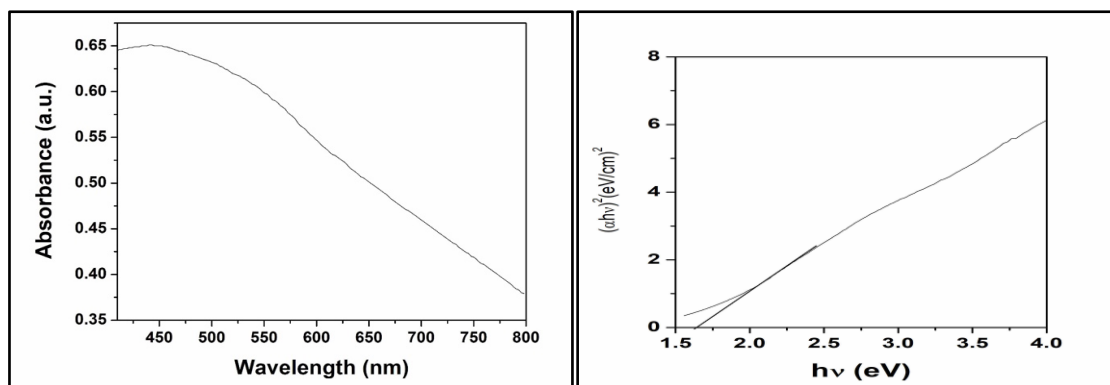


Figure 3.2.3: UV-Vis absorption spectrum and Tauc's plot of nanoparticles of MnFe_2O_4 calcined at $600\text{ }^\circ\text{C}$

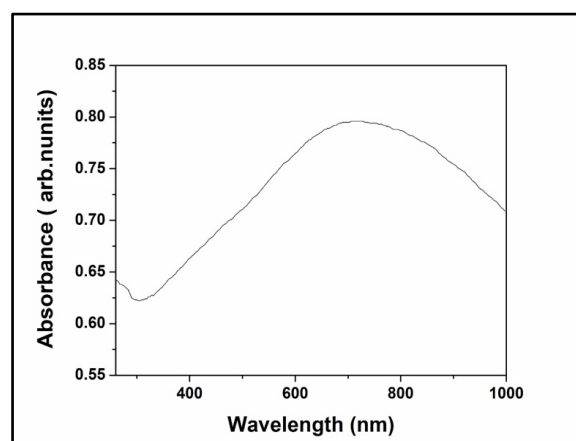


Figure 3.2.4: UV-Visible absorption spectrum of nanoparticles of MnFe_2O_4 calcined at $1000\text{ }^\circ\text{C}$.

3.3 Micro Raman Analysis

The Raman spectrum of MnFe_2O_4 nanoparticles was recorded at room temperature using 532 nm DPSS laser with a maximum power after single mode fiber of around 70 mW in the range $100\text{--}2000\text{ cm}^{-1}$. Raman spectrum of nanoparticles of MnFe_2O_4 calcined at $600\text{ }^\circ\text{C}$ of present study is shown in the figure 3.3.1. The peak position and FWHM of the Raman peak have been obtained by fitting a Lorentzian line shape into the spectrum.

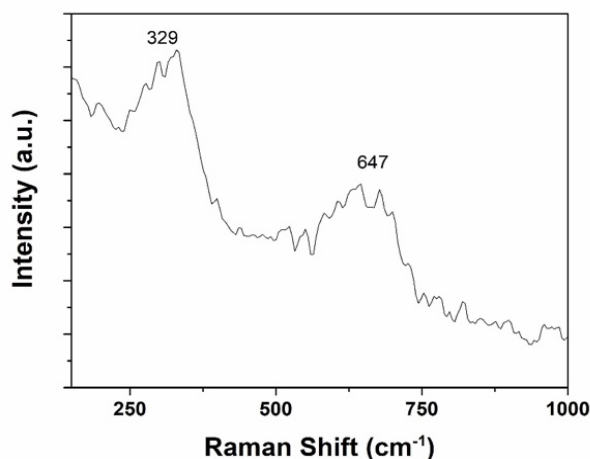


Figure 3.3.1: Raman Spectrum of MnFe₂O₄ nanoparticles calcined at 600^oC

The peak position obtained in the experiment, FWHM and assignment of peaks to different vibrational modes of MnFe₂O₄ is shown in the table. The spectrum showed two Raman bands of MnFe₂O₄.

Table 3.3.1 : Vibrational modes of MnFe₂O₄ nanoparticles calcined at 600^oC

Sl.No.	Peak position (cm ⁻¹)	FWHM (cm ⁻¹)	Assignment
1	329	109	E _g
2	647	102	A _g

4. Conclusion

The CdFe₂O₄ and MnFe₂O₄ nanoparticles synthesized by co-precipitation method were calcined at 600 °C and 1000 °C to study the effect of calcination temperature on the structural and optical properties. From the XRD pattern of the samples, it was observed that both nanoparticles of present study are in cubic phase with normal spinel structure. The grain size of the samples were found to have increased on calcination at high temperature. It was observed that calcination at 1000^oC removed MnO phase in manganese ferrite nanoparticles but CdO peaks were retained in the case of cadmium ferrite. Samples of CdFe₂O₄ calcined at a higher temperature showed significant reduction in strain and dislocation density; but the effect was negligible with MnFe₂O₄. The band gap of nanoparticles of cadmium ferrite and manganese ferrite was found to be blue shifted compared to their bulk counterparts indicating quantum confinement effect. The broad absorption band in the UV- Visible absorption spectrum of manganese ferrite nanoparticles suggests that it can be used as a potential photocatalyst for utilising the whole spectrum of solar radiation rather than being selective of UV radiation. Raman spectrum of the MnFe₂O₄ indicated that the samples of present study were in normal cubic spinel structure, which was in agreement with the XRD pattern. The toxicity studies of

these spinel nanoparticles at cellular and molecular levels and their impact on the environment altogether could be an interesting topic of research on a future note.

Acknowledgements

First author acknowledges DST for providing financial assistance through Women Scientist Scheme-A (SR/WOS-A/PM-96/2018). The corresponding author acknowledges DST-FIST for providing facility in the institution. The authors acknowledge the characterization facilities at CLIF-University of Kerala for XRD studies and SAIF- Mahatma Gandhi University for the Micro-Raman studies.

References

1. Richa Srivastava and Yadav B C. Ferrite Materials: Introduction, Synthesis Techniques, and Applications as Sensors. *International Journal of Green Nanotechnology*. **4.2** (2012) 141-154.
2. Tuyet Nhung Pham, Tran Quang Huy and Anh-Tuan Le. Spinel ferrite (AFe_2O_4)-based heterostructured designs for lithium-ion battery, environmental monitoring, and biomedical applications. *RSC Advances*. **10** (2020) 31622-31661.
3. Galvão W S, Neto D M A, Freire R M and Fechine P B A. Super-Paramagnetic Nanoparticles with Spinel Structure: A Review of Synthesis and Biomedical Applications. *Solid State Phenomena*. **241** (2015) 139–176.
4. Ismail S M, Sh. Labib and Attallah SS. Preparation and Characterization of Nano-Cadmium Ferrite *Journal of Ceramics*. **2013** 526434 (2013) 8 pages.
5. Kefeni K K, Msagati T A M and Mamba B B. Ferrite nanoparticles: synthesis, characterisation and applications in electronic device. *Materials Science and Engineering B*. **215** (2017) 37–55.
6. Pereira C, Pereira AM, Fernandes C, Rocha M, Mendes R F, Fernández-García M P, Guedes A, Tavares PB, Greneche J M, Araújo J P and Freire C. Superparamagnetic MFe_2O_4 (M= Fe, Co, Mn) nanoparticles: tuning the particle size and magnetic properties through a novel one-step coprecipitation route. *Chemistry of Materials*. **24** (2012) 1496–1504.
7. Carta D, Loche D, Mountjoy G, Navarra G and Corrias A. $NiFe_2O_4$ nanoparticles dispersed in an aerogel silica matrix: an X-ray absorption study. *The Journal of Physical Chemistry C*. **112** (2008) 15623–15630.
8. Mukhtar M W, Irfan M, Ahmad I, Ali I, Akhtar M N, Khan M A, Abbas G, Rana M U, Ali A and Ahmad M. Synthesis and properties of Pr-substituted $MgZn$ ferrites for core materials and high frequency applications. *Journal of Magnetism and Magnetic Materials*. **381** (2015) 173–178.
9. Sharma R, Bansal S and Singhal S. Tailoring the photo-Fenton activity of spinel ferrites (MFe_2O_4) by incorporating different cations (M= Cu, Zn, Ni and Co) in the structure. *RSC Advances*. **5** (2015) 6006–6018.
10. Jesudoss S K, Vijaya J J and Kennedy L J and Iyyappa Rajan P. Studies on the efficient dual performance of $Mn_{1-x}Ni_xFe_2O_4$ spinel nanoparticles in photodegradation and antibacterial activity. *Journal of Photochemistry and Photobiology B: Biology*. **165** (2016) 121–132.
11. Tadjarodi A, Imani M and Salehi M. $ZnFe_2O_4$ nanoparticles and a clay encapsulated $ZnFe_2O_4$ nanocomposite: synthesis strategy, structural characteristics and the adsorption of dye pollutants in water. *RSC Advances*. **5** (2015) 56145–56156.
12. Tatarchuk, T., Bououdina, M., Judith Vijaya, J. and John Kennedy, L. Spinel Ferrite Nanoparticles: Synthesis, Crystal Structure, Properties, and Perspective Applications. In: Fesenko, O., Yatsenko, L. (eds) *Nanophysics, Nanomaterials, Interface Studies, and Applications*. NANO 2016. Springer Proceedings in Physics, vol **195**. Springer, Cham 2017.
13. Pang Y L, Lim S and Ong H C and Chong W T. Research progress on iron oxide-based magnetic materials: synthesis techniques and photocatalytic applications. *Ceramics International*. **42** (2016) 9–34.
14. Goswami P P, Choudhury H A, Chakma S and Moholkar V S. Sonochemical synthesis and characterization of manganese ferrite nanoparticles. *Industry & Engineering Chemistry Research*. **52** (2013) 17848–17855.

15. Lai J, Shafi K V P M, Ulman A, Loos K, Yang N L, Cui M H, Vogt T, Estournès C and Locke D C. Mixed iron manganese oxide nanoparticles. *Journal of Physical Chemistry B*. **108** (2004) 14876–14883.
16. Song Q and Zhang Z J. Controlled synthesis and magnetic properties of bimagnetic spinel ferrite CoFe_2O_4 and MnFe_2O_4 nanocrystals with core–shell architecture. *Journal of American Chemical Society*. **134** (2012) 10182–10190.
17. Ni D, Lin Z, Xiaoling P, Xinqing W and Hongliang Ge. Preparation and characterization of nickel-zinc ferrites by a solvothermal method. *Rare Metal Materials and Engineering*. **44** (2015) 2126–2131.
18. Li Z, Gao K, Han G, Wang R, Li H and Guo P. Solvothermal synthesis of MnFe_2O_4 colloidal nanocrystal assemblies and their magnetic and electrocatalytic properties. *New Journal of Chemistry*. **39** (2015) 361–368.
19. Yin Y, Liu W, Huo N and Yang S. Synthesis of vesicle-like MgFe_2O_4 /Graphene 3D network anode material with enhanced lithium storage performance. *ACS Sustainable Chemistry and Engineering*. **5.1** (2017) 563–570.
20. Marinca TF, Chicinas I, Isnard O and Neamtu BV. Nanocrystalline/nanosized manganese substituted nickel ferrites – $\text{Ni}_x\text{Mn}_x\text{Fe}_2\text{O}_4$ obtained by ceramic-mechanical milling route. *Ceramics International*. **42.4** (2016) 4754–4763.
21. Angadi VJ, Rudraswamy B, Sadhana K, Murthy S R and Praveena K. Effect of Sm^{3+} – Gd^{3+} on structural, electrical and magnetic properties of Mn–Zn ferrites synthesized via combustion route. *Journal of Alloys and Compounds*. **656** (2016) 5–12.
22. Singh C, Jauhar S, Kumar V, Singh J and Singhal S. Synthesis of zinc substituted cobalt ferrites via reverse micelle technique involving in situ template formation: a study on their structural, magnetic, optical and catalytic properties. *Materials Chemistry and Physics*. **156** (2015) 188–197.
23. Kotsikau D, Ivanovskaya M and Pankov V and Fedotova Y. Structure and magnetic properties of manganese–zinc-ferrites prepared by spray pyrolysis method. *Solid State Science*. **39** (2015) 69–73.
24. Cortes MS, Martínez-Luevanos A, García-Cerda LA, Rodríguez-Fernández O, Fuentes AF, Romero-García J and Montemayor SM. Nanostructured pure and substituted cobalt ferrites: fabrication by electrospinning and study of their magnetic properties. *Journal of Alloys and Compounds*. **653** (2015) 290–297.
25. Cai X, Wang J and Li B, Wu A, Xu B, Wang B, Gao H, Yu L and Li Z. Microwave absorption properties of LiZn ferrites hollow microspheres doped with La and Mg by self-reactive quenching technology. *Journal of Alloys and Compounds*. **657** (2016) 608–615.
26. Ishaque M, Khan M A, Ali I, Khan H M, Iqbal MA, Islam M U and Warsi M F. Investigations on structural, electrical and dielectric properties of yttrium substituted Mg-ferrites. *Ceramics International*. **41.3** (2015) 4028–4034.
27. Anjum S, Hameed S and Bashir F. Microstructural, structural, magnetic and optical properties of antimony doped cobalt spinel ferrites. *Materials Today Proceedings* **2.10 B** (2015) 5329–5336.
28. Cross W B, Affleck L, Kuznetsov M V and Ivan P. Self-propagating high-temperature synthesis of ferrites MFe_2O_4 (M=Mg, Ba, Co, Ni, Cu, Zn); reactions in an external magnetic field. *Journal of Materials Chemistry*. **9** (1999) 2545–2552.
29. Peng E, Ding J and Xue J M. Concentration-dependent magnetic hyperthermic response of manganese ferrite-loaded ultrasmall graphene oxide nanocomposites. *New Journal of Chemistry* **38** (2014) 2312–2319.
30. Leal MP, Rivera-Fernández S, Franco JM, Pozo D, de la Fuente JM, García-Martín ML. Long-circulating PEGylated manganese ferrite nanoparticles for MRI-based molecular imaging. *Nanoscale* **7** (2015) 2050–2059.
31. Linfeng Zhang and Yuanxin Wu. Sol-Gel Synthesized Magnetic Spinel Ferrite Nanoparticles as Novel Catalyst for Oxidative Degradation of Methyl Orange. *Journal of Nanomaterials*. **2013** 640940 (2013)6 pages.
32. Kaiser M. Magnetic and electric modulus properties of In substituted Mg–Mn–Cu ferrites. *Material Research Bulletin*. **73** (2016) 452–458.

33. Patil S.B, Bhojya Naik HS, Nagaraju G, and Yallappa Shiralgi. Sugarcane juice facilitated eco-friendly synthesis of solar light active CdFe₂O₄ nanoparticles and its photocatalytic application. *The European Physics Journal Plus*. **133** (2018) 229.
34. Cullity B D. Elements of X-ray diffraction, II Edition, Addison-Wesley Publishing Company, Massachusetts. 1978.
35. Chipera S J and Bish D L. Applications of X-Ray Diffraction Crystallite Size/Strain Analysis to Seismosaurus Dinosaur Bone. *Advances in X-Ray Analysis*. **34** (1991) 473-482.
36. Savaloni, Shahraki M G and Player MA. A comparison of different methods for X-ray diffraction line broadening analysis of Ti and Ag UHV deposited thin films: nanostructural dependence on substrate temperature and film thickness. *Journal of Physics D: Applied Physics*. **39**.10 (2006) 2231-2247.
37. Nayak P K. Synthesis and characterization of cadmium ferrite. *Materials Chemistry and Physics*. **112** (2008) 24-26.
38. Gaba S., Rana P S., Kumar A. and Pant R P. Structural and paramagnetic resonance properties correlation in lanthanum ion doped nickel ferrite nanoparticles. *Journal of Magnetism and Magnetic Materials*. **508** (2020) 166866.
39. Suryanarayana C and Grant Norton M, X-ray Diffraction: A Practical Approach. Springer, New York, 1998.
40. Anayara Begum, Amir Hussain and Atowar Rahman. Effect of deposition temperature on the structural and optical properties of chemically prepared nanocrystalline lead selenide thin films. *Beilstein Journal of Nanotechnology*. **3** (2012) 438-443.
41. Ma E, Shen T D and Wu X L. Nanostructured metals: less is more. *Nature Materials*. **5**.7 (2006) 515-516.
42. Tong X., Zhang H. and Li D. Effect of Annealing Treatment on Mechanical Properties of Nanocrystalline α -iron: an Atomistic Study. *Scientific Reports*. **5** (2015) 8459-8462.
43. Murray C B, Norris D J, and Bawendi MG. Synthesis and characterization of nearly monodisperse CdE (E = sulfur, selenium, tellurium) semiconductor nanocrystallites. *Journal of American Chemical Society*. **115**.19 (1993) 8706-8715.
44. Kayanuma Y. Quantum-size effects of interacting electrons and holes in semiconductor microcrystals with spherical shape. *Physical Review B*. **38**.14 (1988) 9797-9805.
45. Wang Y and Herron N. Nanometer-sized semiconductor clusters: materials synthesis, quantum size effects, and photophysical properties. *Journal of Physical Chemistry*. **95**.2 (1991) 525-532.
46. Brus L E, and Trautman JK, Nanocrystals and nano-optics. *Philosophical Transactions of the Royal Society of London. Series A: Physical and Engineering Sciences*. **353**.1703 (1995) 313-321.
47. Sugak D, Syvorotka II, Yakhnevych U, Buryy O, N. Martynyuk N, Ubizskii S, Ya. Zhydachevskyy, Suchocki A, Kumar H, V. Janyani V and Singh G. Optical Investigation of the Cu Ions Diffusion into Bulk Lithium Niobate. *Acta Physica Polonica A*. **133**.4 (2018) 965-972.